Journal of Molecular Graphics and Modelling 30 (2011) 186–197

Contents lists available at ScienceDirect

Journal of Molecular Graphics and Modelling

journal homepage: www.elsevier.com/locate/JMGM

Pharmacophore filtering and 3D-QSAR in the discovery of new JAK2 inhibitors

Kh. Dhanachandra Singh, Muthusamy Karthikeyan*, Palani Kirubakaran, Selvaraman Nagamani

Department of Bioinformatics, Alagappa University, Karaikudi 630 003, Tamil Nadu, India

ARTICLE INFO

Article history:
Received 12 May 2011
Received in revised form 13 July 2011
Accepted 14 July 2011
Available online 22 July 2011

Keywords:
JAK2
Pharmacophore
3D-QSAR
Docking

ABSTRACT

Janus kinase 2 (JAK2) plays a crucial role in the patho-mechanism of cardiovascular pathologies, myeloproliferative disorders and many other diseases. Thus, effective JAK2 kinase inhibitors may be of significant therapeutic importance. In this study, a pharmacophore mapping studies were undertaken for a series of phenylaminopyrimidines derivatives. A five point pharmacophore with two hydrogen bond donors (D), two hydrogen bond acceptors (A) and one aromatic ring (R) as pharmacophoric features were developed. The pharmacophore hypothesis yielded a statistically significant 3D-QSAR model, with a correlation coefficient of $R^2 = 0.970$ for training set compounds. The model generated showed excellent predictive power, with a correlation coefficient of $Q^2 = 0.822$. The external validation indicated that our QSAR models possessed high predictive powers with r_0^2 value of 0.999 and r_m^2 value of 0.637 respectively. The model was then employed as 3D search query to screen against public compound libraries (Asinex, TOSLab, Maybride and Binding database) in-order to identify a new scaffold. We have identified thirteen distinct drug-like molecules binding to the JAK2. Interestingly, some of the compounds show activity against JAK2 by PASS biological activity prediction. Hence, these molecules could be potential selective inhibitors of JAK2 that can be experimentally validated and their backbone structural scaffold could serve as building blocks in designing drug-like molecules for JAK2.

1. Introduction

Janus tyrosine kinase 2 (JAK2) is a member of the Janus family of tyrosine kinases and it is important in many of cellular signaling pathways [1–3]. After the discovery of JAK2 in 1991, it has been shown to be activated by a wide variety of receptors including cytokine receptors, growth factor receptors, and seven transmembrane-spanning receptors [1]. The Janus-associated kinase (JAK) family consists of four non-receptor tyrosine kinases (JAK1, JAK2, JAK3, and TYK2) that play pivotal roles in many aspects of cytokine and growth factor mediated signal transduction [4–6]. JAK2 is essential for hematopoiesis, platelet formation and other functions that are important in cellular survival, proliferation and differentiation [2]. The JAKs play critical roles in several important intracellular signaling pathways, including the eponymous JAK/STAT pathway, central to the mediation of cytokine signaling [3]. Somatic mutation of JAK2 (V617F), has recently been identified in patients with polycythemia vera, essential thrombocytosis [7] and myelofibrosis [4], hematopoietic malignancies, including auto-immune diseases, myeloproliferative syndromes [8–11] leukemias [12,13] and lymphomas [14] as well as cardiovascular disease [15]. This mutation results in a constitutively active JAK2 tyrosine kinase. Currently, this remains an area of intense research to understand the exact mechanism by which the JAK2 kinase is activated via the valine to phenylalanine substitution at position 617.

JAK2 has been linked to similar cardiovascular pathologies as have been previously linked to the renin–angiotensin system. Identifying the downstream targets of JAK2 *via* the angiotensin II type 1 (AT1) receptor may therefore elucidate its role in the progression of various pathologies [1]. Through mechanisms that are not yet fully understood but probably involve Ca^{2+} and possibly PYK2 kinase or SRC kinase, angiotensin II also activates intracellular JAK2. JAK2 then phosphorylates and activates Arhgef1, which stimulates the RhoA-Rho kinase–myosin phosphatase target subunit (MYPT) cascade, inhibiting myosin light chain phosphatase (MLCP), which has the effect of promoting phosphorylation of myosin light chain (MLC) and ultimately increases blood pressure. Guilluy et al. show that, in the absence of functional JAK2 within smooth muscle cells, angiotensin II will not induce hypertension [16]. Thus, effective JAK2 kinase inhibitors may be of significant therapeutic importance [17].

In the present study, PHASE (Schrodinger, LLC), was used to develop pharmacophore modeling, 3D-QSAR model and database screening. Ligand-based drug design approaches like pharmacophore mapping and QSAR can be used in the discovery of new lead compounds [18]. Here we describe the development of robust ligand based 3D-pharmacophore hypothesis using pharmacophore

* Corresponding author. Tel.: +91 4565 230725; fax: +91 4565 225202.
E-mail address: mkbioinformatics@gmail.com (M. Karthikeyan).

1093-3263/$ – see front matter © 2011 Elsevier Inc. All rights reserved.
doi:10.1016/j.jmgm.2011.07.004

Table 1
Compounds selected (4-aryl substituent) for 3D-QSAR study and their measured biological activity and predicted activity.

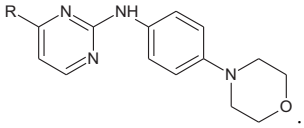

Compound No.	R	PIC_{50} valueExperimental	PIC_{50} valuePredicted	Residual	Dataset
1	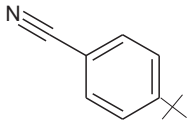	6.273	6.23	0.043	Training
2	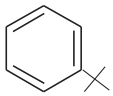	6.331	6.47	−0.139	Training
3	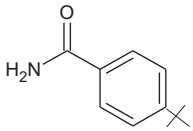	6.487	6.86	−0.373	Test
4	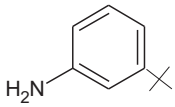	6.492	6.5	−0.008	Training
5	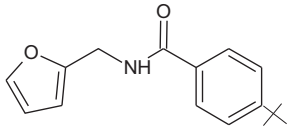	6.695	6.53	0.165	Test
6	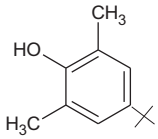	7.056	7.2	−0.144	Test
7	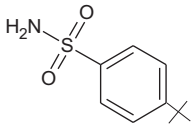	7.08	7.06	0.02	Training
8	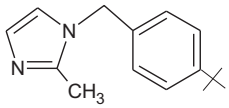	7.092	6.8	0.292	Training
9	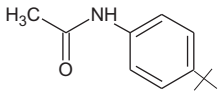	7.174	7.36	−0.186	Training
10	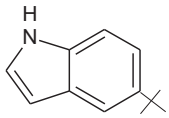	7.481	7.32	0.161	Training
11	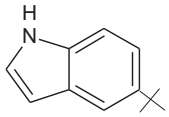	7.796	7.96	−0.164	Training
12	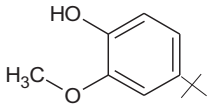	8.523	8.57	−0.047	Training

Table 2
Compounds selected (N-phenylmethanesulfonamide) for 3D-QSAR study and their measured biological activity and predicted activity.

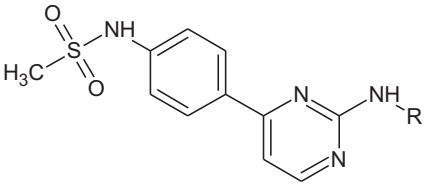

Compound	R	PIC_{50} valueExperimental	PIC_{50} valuePredicted	Residual	Dataset
13	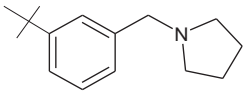	8.222	8.15	0.072	Test
14	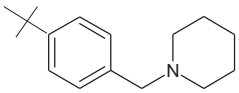	7.959	7.83	0.129	Test
15	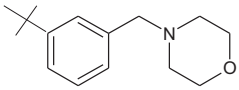	8.097	8.18	−0.083	Training
16	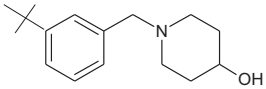	7.921	8.09	0.011	Training
17	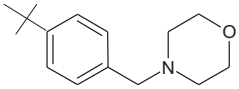	8.046	7.89	0.156	Training
18	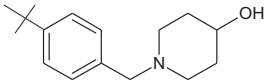	7.796	7.75	0.046	Training
19	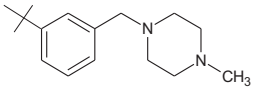	7.854	8.04	−0.186	Training
20	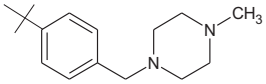	7.745	7.91	−0.165	Test
21	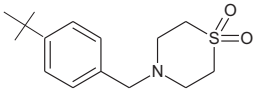	8.699	8.69	0.009	Training
22	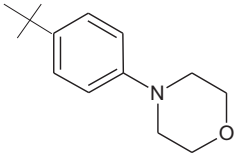	8.398	7.93	0.468	Test
23	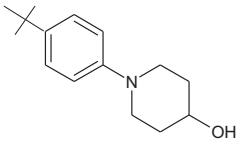	8.222	8.12	0.102	Training

alignment and scoring engine for JAK2 inhibitors. The alignment obtained from the pharmacophoric points was used to derive an atom-based 3D-QSAR model. The pharmacophore thus developed imparts information about important features for JAK2 inhibitory activity and geometry, and it was used to mine 3D-virtual databases of drug-like molecules. The contours generated from QSAR studies highlight the structural features required for JAK2 inhibition and it will be useful for further design of more potent inhibitors.

2. Materials and methods

2.1. Computational details

PHASE 3.2 implemented in the Maestro 9.1 software package (Schrodinger, LLC) [20–22] was used to generate pharmacophore and 3D-QSAR models for phenylaminopyrimidines derivatives as inhibitors of JAK2. A dataset comprising 43

Table 3
Compounds selected (nitrile carboxamide) for 3D-QSAR study and their measured biological activity and predicted activity.

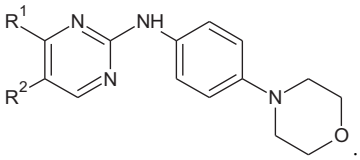

Compound	R^1	R^2	PIC_{50} valueExperimental	PIC_{50} valuePredicted	Residual	Dataset
24	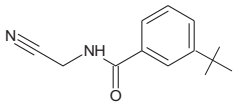	H	6.264	6.17	0.094	Training
25	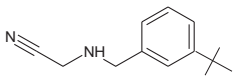	H	6.519	6.51	0.009	Training
26	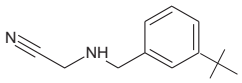	H	6.879	6.73	0.149	Test
27	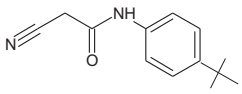	H	8	7.91	0.09	Training
28	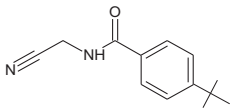	H	7.745	7.64	0.105	Training
29	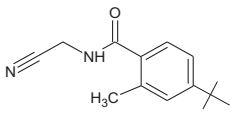	H	7.187	7.34	−0.153	Test
30	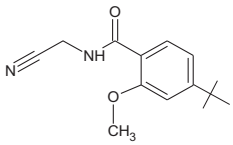	H	7.523	7.64	−0.117	Training
31	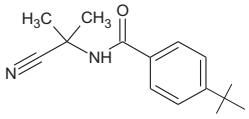	H	6.26	6.44	−0.18	Training
32	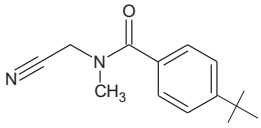	H	6.526	6.43	0.096	Training
33	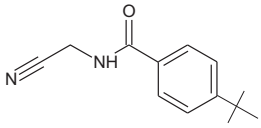	Me	8.097	7.83	0.267	Training
34	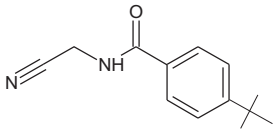	OMe	6.73	6.87	−0.14	Training

phenylaminopyrimidines derivatives were selected from available literature [19] and were used in the present study. Table 1 shows the 4-aryl substituent (compound 1–12), Table 2 shows the N-phenylmethanesulfonamide series (compound 13–23), Table 3 shows the nitrile carboxamide series (compound 24–34) and Table 4 shows the N-cyanomethylbenzamide series (compound 35–43). From the total 43 molecules, 31 of these were randomly chosen for training set and 12 were selected as test set (Tables 1–4), by using the "Automated Random Selection" option present in the PHASE software. PHASE provides a built-in set of six pharmacophore features, hydrogen bond acceptor (A), hydrogen bond donor (D), hydrophobic group (H), negatively ionizable (N), pos-

Table 4
Compounds selected (N-cyanomethylbenzamide) for 3D-QSAR study and their measured biological activity and predicted activity.

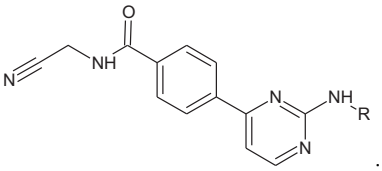

Compound	R	PIC_{50} value Experimental	PIC_{50} value Predicted	Residual	Dataset
35	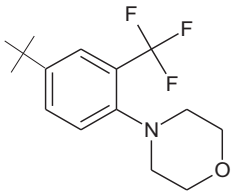	6.427	6.48	−0.053	Training
36	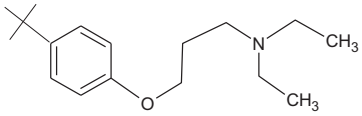	6.78	6.8	−0.02	Training
37	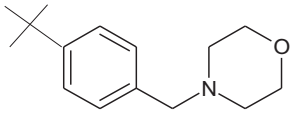	6.788	6.99	−0.202	Test
38	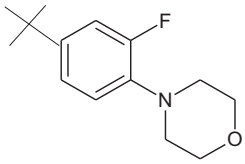	6.936	7.34	−0.404	Test
39	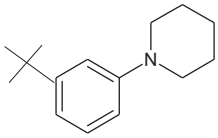	6.947	7.07	−0.123	Training
40	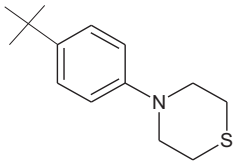	7.161	7.13	0.031	Training
41	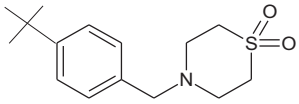	7.284	7.39	−0.106	Training
42	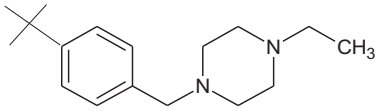	7.328	7.32	0.008	Training
43	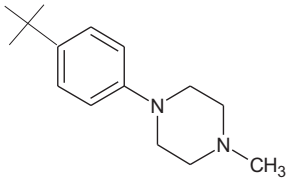	7.387	7.11	0.277	Test

itively ionizable (P), and aromatic ring (R). The pharmacophore model was developed using a set of pharmacophore features to generate sites for all the compounds [23]. For QSAR development, pharmacophore models of training set molecules were placed into regular grid of cubes, with each cube allotted zero or more "bits' to account for the different type of pharmacophore features in the training set that occupy the cube (1 Å). This representation gives rise to binary-valued occupation patterns that can be used as independent variables to create partial least-squares (PLS) factors 3D-QSAR models.

Table 5
Summary of quantitative structure activity relationship (QSAR) result for the five best common pharmacophore hypotheses.

Hypotheses No.	Hypothesis	SD	R^2	F	r^2_{pred}	RMSE	Q^2	Pearson-R
1	AADDR	0.136	0.970	206.100	0.820	0.254	0.822	0.911
2	ADDRR	0.156	0.960	154.400	0.731	0.313	0.731	0.865
3	ADRRR	0.183	0.944	110.200	0.652	0.355	0.653	0.873
4	DDRRR	0.123	0.975	253.000	0.592	0.387	0.588	0.791
5	AADRR	0.205	0.931	287.200	0.673	0.345	0.673	0.829

SD: Standard deviation of the regression, r^2 for the regression, F variance ratio, r^2_{pred} for the predictive r^2, p significance level of variance ratio, RMSE root mean square error. q^2 value of q^2 for the predicted activities. Pearson R correlation between the predicted and observed activity for the test set.

Table 6
Analyses of critical amino acids for Jak2 inhibition from 10 co-crystal structures deposited in protein data bank.

PDB ID	Leu855	Gly856	Lys857	Val863	Ala880	Met929	Glu930	Leu932	Asn981	Leu983	Asp994
2B7A	√	√	√	√	√	√	√	√	X	√	X
3E62	×	×	×	√	√	√	√	√	×	√	×
3E63	√	√	√	√	√	√	√	√	×	√	×
3E64	√	√	×	√	√	√	√	√	√	√	√
3FUP	√	×	√	√	√	×	√	√	×	√	√
3IO7	√	×	√	√	√	√	×	√	√	√	√
3IOK	√	√	√	×	√	√	×	√	×	√	√
3JY9	√	√	×	√	√	√	√	√	×	√	√
3KC	√	×	×	√	√	√	√	√	×	√	√
36PB	√	×	×	√	√	√	×	√	×	√	×

2.2. PLS analysis and validation

The predictive value of the models was evaluated by leave-one-out (LOO) and leave-half-out (LHO) cross-validation. The cross validated coefficient, r^2_{cv}, was calculated using the following equation:

$$r^2_{cv} = 1 - \frac{\sum(Y_{predicted} - Y_{observed})^2}{\sum(Y_{observed} - Y_{mean})^2} \quad (1)$$

where

$Y_{predicted}$, $Y_{observed}$, and Y_{mean} are the predicted, observed, and mean values of the target property (pIC_{50}), respectively.
$(Y_{observed} - Y_{mean})^2$ is the predictive residual sum of squares (PRESS).

The predictive correlation coefficient (r^2_{pred}), based on molecules of test set, is defined as,

$$r^2_{pred} = \frac{\text{SD} - \text{PRESS}}{\text{SD}} \quad (2)$$

where SD is the sum of the squared deviations between the biological activities of the test set and mean activities of the training set molecules and PRESS is the sum of squared deviation between predicted and actual activity values for every molecule in test set [24].

2.3. External validation

To evaluate the true predictive abilities of the established models, it is necessary to perform external validation. According to literature [25–27], 3D-QSAR models were accepted if they satisfy all of the following conditions:

$$r^2_{cv} > 0.5, r^2 > 0.6, \left[\frac{r^2 - r^2_o}{r^2}\right] < 0.1, 0.85 \le k \le 1.15$$

and $r^2_m > 0.5$.

The r^2 value calculated by the following formula:

$$R = \frac{\sum(y_i - \bar{y}_o)(\tilde{y}_i - \bar{y}_p)}{\sqrt{\sum(y_i - \bar{y}_o)^2 \sum(\tilde{y}_i - \bar{y}_p)^2}} \quad (3)$$

In these equations, y_i and $\tilde{y}_i$ are the observed and predicted activity, $\bar{y}_o$ and $\bar{y}_p$ are the average values of the observed and predicted pIC_{50} values of the test set molecules. For the ideal QSAR model, the r^2 value should be close to 1. Meanwhile the regression

Table 7
Summary of docking and fitness results for thirteen best lead molecules.

Lead molecule	Glide score	Glide energy (kcal/mol)	Align score	Volume score	Fitness	ΔG_{bind} (kcal/mol)	Interacting residue
Lead 1	−13.869	−61.850	0.280	0.479	2.197	−19.599	Leu932, Asn981
Lead 2	−13.752	−62.310	0.310	0.394	2.015	−17.650	Leu932, Asn981
Lead 3	−13.679	−64.856	0.281	0.487	2.203	−8.262	Leu932, Asn981
Lead 4	−13.540	−61.943	0.280	0.489	2.206	−12.283	Leu932, Asn981
Lead 5	−13.418	−54.758	0.452	0.421	1.826	−65.157	Leu932, Asp939, Leu855
Lead 6	−13.343	−60.545	0.294	0.453	2.172	−2.023	Leu932, Asp994, Asn981
Lead 7	−13.081	−58.321	0.743	0.413	1.735	−3.353	Tyr931, Arg980, Asp976, Asp994
Lead 8	−13.033	−59.057	0.625	0.403	1.833	−9.545	Leu932, Asn981, Arg980
Lead 9	−12.987	−68.511	0.760	0.300	1.590	−57.209	Leu932, Asn981, Lys882
Lead 10	−12.841	−56.716	0.651	0.442	1.748	−3.259	Tyr931, Leu855, Arg980, Asp976, Asp994
Lead 11	−12.763	−52.873	0.531	0.418	1.892	−77.658	Tyr931, Asp939
Lead 12	−12.729	−49.604	0.914	0.458	1.575	−70.152	Leu932, Asp939, Gly993
Lead 13	−12.688	−49.581	0.918	0.443	1.536	−65.685	Leu932, Asp939, Gly993
Azd1480[a]	−9.186	−33.653	0.568	0.417	1.800	−66.894	Leu932, Glu930

[a] AZD1480 is a potential JAK2 inhibitor which used as a reference compound.

Table 8
Docking score and binding energy of the compounds selected for QSAR study.

Compound No.	Docking score	Glide energy (kcal/mol)	ΔG_{bind} (kcal/mol)	Interacting residue
1	−10.731	−46.009	−17.576	Leu932
2	−10.578	−40.148	−11.193	Leu932
3	−10.471	−48.146	−12.536	Leu932, Asp994
4	−11.404	−43.395	−8.858	Leu932, Leu855
5	−11.809	−54.623	−17.834	Leu932, Asp994
6	−10.839	−38.631	2.632	Leu932, Asp994
7	−10.656	−46.896	−78.942	Leu932
8	−11.215	−52.983	−88.261	Leu932
9	−11.075	−46.409	−15.649	Leu932, Asp994
10	−10.989	−49.397	−54.568	Leu932, Leu855
11	−11.157	−38.112	−1.2538	Leu932, Leu855
12	−11.495	−37.439	−8.132	Leu932, Leu855
13	−11.913	−49.348	−76.633	Leu932, Asp939, Asp994
14	−10.912	−52.590	−64.906	Leu932, Asp994
15	−11.438	−49.049	−10.410	Leu392, Asp994
16	−11.738	−45.053	−72.069	Leu932, Asp939, Asp994
17	−11.571	−53.062	0.789	Leu932, Asp994
18	−11.967	−52.569	−63.461	Leu932, Asp994
19	−11.866	−51.538	−78.079	Leu932, Asp994, Asp939
20	−12.207	−50.758	−66.372	Leu932, Asp994
21	−11.786	−49.898	−74.759	Leu932, Asp994, Asp939
22	−11.438	−49.047	−14.839	Leu932, Asp994
23	−11.447	−54.665	−13.717	Leu932, Asp994, Asp939
24	−10.919	−48.561	−8.583	Leu932
25	−11.131	−51.219	−10.917	Leu932, Leu855
26	−11.573	−49.061	−68.994	Leu932, Arg980
27	−11.673	−48.949	−11.978	Leu932, Asp994, Arg980
28	−11.477	−52.814	−10.412	Leu932, Asp994, Arg980
29	−11.250	−53.003	−6.482	Leu932, Arg980
30	−11.178	−52.326	−2.816	Leu932, Arg980
31	−11.313	−53.887	0.614	Leu932, Arg980
32	−10.916	−45.017	−6.397	Leu932, Arg980
33	−11.758	−54.216	−15.324	Leu932, Asp994, Arg980
34	−10.824	−53.338	−10.142	Leu932, Arg980
35	−11.643	−43.996	−15.691	Leu932, Glu930, Ser936, Arg980
36	−11.859	−59.405	−79.397	Leu932, Leu855, Gly993, Arg980, Asp994
37	−12.086	−56.377	−8.285	Leu932, Gly993, Asp994
38	−11.839	−53.545	−3.699	Leu932, Asp994, Arg980
39	−11.862	−47.185	−80.380	Leu932, Gly993
40	−11.697	−56.552	−7.692	Leu932, Arg980, Asp994
41	−10.979	−54.347	−44.620	Leu932, Gly993, Asp994, Arg980
42	−12.260	−58.955	−69.963	Leu932, Gly993, Asp994
43	−12.208	−56.137	−76.700	Leu932, Gly993, Asp994, Arg980

of y against $\bar{y}$ through origin: $y_i^{ro} = k\tilde{y}_i$ should be characterized by k close to 1. Slope k is calculated as follow:

$$k = \frac{\sum y_i \tilde{y}_i}{\sum \tilde{y}_i^2} \quad (4)$$

Another essential parameter r_m^2 was defined as follow:

$$r_m^2 = r^2 \left(1 - \sqrt{\left|r^2 - r_o^2\right|}\right) \quad (5)$$

Table 9
ADME properties of the thirteen lead molecules by using QikProp, Schrodinger 9.1.

Lead molecules	QPlogPo/w[a]	QPlogS[b]	QPlogHERG[c]	QPPCaco[d]	QPPMDCK[e]	Percent human oral absorption[f]
Lead 1	4.333	−6.700	−7.700	558.551	476.558	100.000
Lead 2	4.538	−7.069	−7.710	487.528	561.261	100.000
Lead 3	4.147	−6.732	−7.250	509.126	588.185	100.000
Lead 4	4.354	−6.889	−7.699	489.918	228.776	100.000
Lead 5	3.526	−4.177	−5.335	812.195	875.358	100.000
Lead 6	5.227	−7.802	−7.602	620.674	728.636	94.581
Lead 7	1.555	−3.669	−6.048	124.609	52.089	73.555
Lead 8	5.303	−8.092	−7.482	598.721	2955.977	81.787
Lead 9	3.312	−4.219	−8.181	69.374	74.665	79.292
Lead 10	0.834	−3.102	−5.275	62.460	24.691	63.966
Lead 11	3.763	−5.682	−6.274	805.138	391.388	100.000
Lead 12	3.636	−4.869	−6.229	298.676	204.039	92.537
Lead 13	3.520	−4.816	−6.436	299.882	148.893	91.890

[a] Predicted octanol/water partition co-efficient log p (acceptable range: −2.0 to 6.5).
[b] Predicted aqueous solubility; S in mol/L (acceptable range: −6.5 to 0.5).
[c] Predicted Caco-2 cell permeability in nm/s (acceptable range: <25 is poor and >500 is great).
[d] Predicted apparent MDCK cell permeability in nm/s.
[e] Predicted IC50 value for blockage of HERG K+ channels (concern below −5.0).
[f] Percentage of human oral absorption (<25% is poor and >80% is high).

where r^2 was the non-cross-validated correlation coefficient obtained from the PLS process, and the r_o^2 was calculated as follows:

$$r_o^2 = 1 - \frac{\sum \left(\tilde{y}_i - y_i^{ro}\right)^2}{\sum (\tilde{y}_i - \bar{y}_p)^2} \quad (6)$$

The y_i^{ro} was obtained by this formula:

$$y_i^{ro} = k\tilde{y}_i \quad (7)$$

The best predicted pharmacophore were subjected to screen against large public compound libraries from Asinex (www.asinex.com), Maybridge (www.maybridge.com), TOSLab (www.toslab.com), Binding database (www.bindingdb.org/bind/index.jsp).

The crystal structure of JAK2 (PDB id: 3E64) was downloaded and prepared in protein preparation wizard of Schrodinger, LLC, 2010. The rigid receptor docking using the Glide program [28] was carried out against the receptor using the same set of ligands. Glide provides three different level of docking precision (HTVS, high throughput virtual screening; SP, standard precision, XP, extra precision). We carried out our calculations in HTVS first, then in SP and XP mode for further refinement of good ligand pose.

Prime/MM-GBSA is used to predict the free energy of binding for set of ligands to receptor. The binding free energy (ΔG_{bind}) is then estimated using equation:

$$\Delta G_{\text{bind}} = E_{\text{R:L}} - (E_{\text{R}} + E_{\text{L}}) + \Delta G_{\text{solv}} + \Delta G_{\text{SA}} \quad (8)$$

where $E_{\text{R:L}}$ is energy of the complex, $E_{\text{R}} + E_{\text{L}}$ is sum of the energies of the ligand and apo protein, using the OPLS-2005 force field, ΔG_{solv} (ΔG_{SA}) is the difference between GBSA solvation energy (surface area energy) of complex and sum of the corresponding energies for the ligand and apo-protein [29].

2.4. Biological activity spectrum (BAS)

Biological activity spectrum (BAS) of a compound represents the complex of pharmacological effects, physiological and biochemical mechanisms of action, specific toxicity (mutagenicity, carcinogenicity, teratogenicity and embryotoxicity) which can be revealed in compound's interaction with biological system [30]. The set of pharmacological effects, mechanisms of action, and specific toxicities that might be exhibited by a particular compound in its interaction with biological entities are predicted by PASS and it is termed as "biological activity spectrum" of the compound [31]. We further analyzed the ADME properties of the screened compounds using QikProp program [32,33].

3. Result and discussion

3.1. Determination of pharmacophore and 3D-QSAR models

To find the common pharmacophore hypothesis, the dataset were divided into active and inactive sets. Molecules with pIC_{50} values higher than 8.00 were considered to be active and those with pIC_{50} values less than 6.6 were considered to be inactive, whereas those pIC_{50} values in-between were considered to be moderately active. Reference relative conformational energy (kJ/mol) was included in the score, and ligand activity, expressed as pIC_{50} was incorporated with a default weight. Hypotheses emerging from this process were subsequently scored with respect to the nine inactive, using a weight of 1.0. The hypotheses that survived the scoring process were used to build an atom based QSAR model.

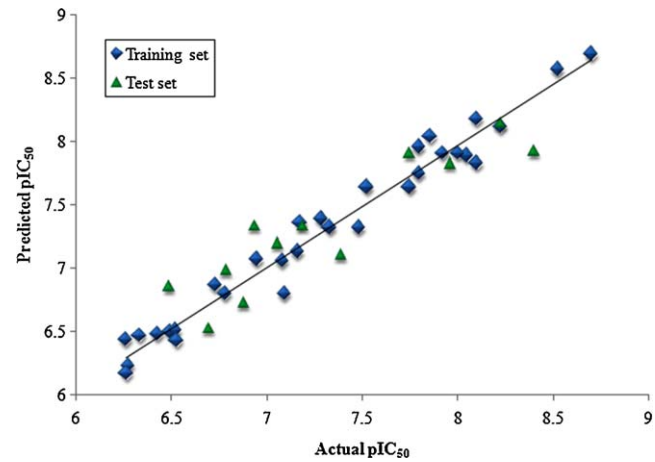

Fig. 1. Graph of actual versus predicted pIC_{50} of the training set and the test set using atom based QSAR model from PHASE.

3.2. Analysis of phase 3D-QSAR validation

Reliable predictions can only come from statistically valid QSAR model [34]. There are several statistical parameters, such as leave-n-out cross validation for training set (R^2), leave-n-out cross validation for test set (Q^2), standard deviation (SD), Root Mean Square Error (RMSE), and variance ratio (F) that can be used to evaluate the robustness of a QSAR model. As shown in Table 5, the Q^2 value of all the hypotheses are greater than 0.55, the SD values are lower than 0.3, and the F-test values are very high. High R^2 is necessary but not sufficient condition for a predictive QSAR model [25,35]. Besides the consideration of high R^2, the best QSAR model should be chosen based on its predictive ability, so the best model should have high Q^2 also. Good and consistent external predictivity was observed in hypothesis 1 for each combination as compared to others. Hypothesis 1 shows a good R^2 value for the training set (0.970), excellent predictive power with Q^2 of 0.822, lowest RMSE (0.254) and goodness of the model was predicted by r^2_{pred} for test set (0.820) as shown in Table 5.

3.3. Analysis of external validation

The established QSAR model using twelve molecules in the test set, gave an excellent r^2_{cv} value of 0.969 (>0.5), r^2_m value of 0.637 (>0.5) as well as high slope of regression lines through the origin (k) value of 0.998 ($0.85 \le k \le 1.15$), and the non-cross validated correlation coefficient (r^2) values of 0.910 (close to 1), and the calculated ($r^2 - r_o^2/r^2$) values of −0.099 (<0.1) were obtained. The results of the external validation indicated that the QSAR models possessed a high accommodating capacity; they may be reliable for being used to predict the activities of new derivatives. Plots of predicted vs. actual pIC_{50} for training and test set are shown in Fig. 1. Hence the hypothesis 1 with two hydrogen bond acceptors (A), two hydrogen bond donors (D) and one aromatic ring (R) as pahrmacophoric feature was retained for further QSAR studies. The distance between the pharmacophoric features are depicted in Fig. 2 and Supplementary Table 2. In the pharmacophore mapping study, it was found that the major structural factors, affecting the potency of these compounds, are related to the basic scaffold. The two hydrogen bond donor sites, together with the acceptor sites, reflect the importance of the H-bonding and were consistent with the crystallographic structure 3E64.

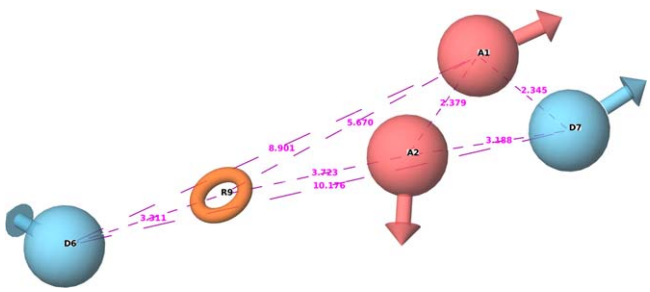

Fig. 2. Pharmacophore hypothesis and distance between the pharmacophoric sites. All the distances are in Å unit.

3.4. Analysis of binding site

Ten co-crystallized crystal structures of JAK2 were deposited in protein data bank (http://www.pdb.org/pdb/home/home.do). PDB id 3E64 was selected for this study base on their resolution (Supplementary Table 1). Binding site was defined using the critical amino acids which were identified by analyzing the protein–ligand interactions from the ten JAK2 co-crystal structures which were deposited in PDB. All the ligands in the complex structures showed the hydrogen bond and hydrophobic interactions with Leu855, Gly856, Lys857, Val863, Ala880, Met929, Glu930, Leu932, Asn981, Leu983, and Asp994 (Table 6).

3.5. Pharmacophore-based virtual screening

The database search studies retrieved all the positive hits and filtered out the inactive compounds. Interpretation of how the pharmacophore maps onto the positive hits can provide an insight into the structural requirements for inhibition of JAK2, and can act as a guide for further modification of the molecules. The generated pharmacophore model was used to screen against the public databases of 294,895 compounds (Asinex, Binding database, TOSLab, Maybridge). The compounds which posses the fitness scores more than 1.500 (1654 compounds) were placed for High throughput virtual screening. Through HTVS, we identified 382 ligands which bind to the active site of JAK2. For further refinement we placed these compounds for Glide SP docking. 215 compounds were filtered out from Glide SP and further proceeded for more precise Glide XP docking study. Finally we identified 13 ligands which interact to the active site residues of JAK2. All the five pharmacophore hypotheses sites are present in our identified compounds.

The chemical name of the thirteen lead compounds with their corresponding Binding database identity (ID) numbers are (S)-N-{1-(3-Fluorophenyl)-2-hydroxyethyl}-4-{5-methyl-2-(phenylamino)pyrimidin-4-yl}-1H-pyrrole-2-carboxamide (*Lead 1: 35649*), (S)-N-{1-(3-Chlorophenyl)-2-hydroxyethyl}-4-{5-methyl-2-(phenylamino)pyrimidin-4-yl}-1H-pyrrole-2-carboxamide (*Lead 2: 35650*), (S)-4-{2-(Benzo[d]1,3-dioxolylamino)-5-methylpyrimidin-4-yl}-N-{1-(3-chlorophenyl)-2-hydroxyethyl}-1H-pyrrole-2-carboxamide (*Lead 3: 35662*), (S)-N-{1-(3-Methylphenyl)-2-hydroxyethyl}-4-{5-methyl-2-(phenylamino)pyrimidin-4-yl}-1H-pyrrole-2-carboxamide (*Lead 4: 35651*), 4-(2-((2-(1H-imidazol-4-yl)ethyl)amino)pyridin-4-yl)-N-(3-chlorophenyl)pyrimidin-2-amine (*Lead 5: 11322*), (S)-4-{2-(2-Ethylphenylamino)-5-methylpyrimidin-4-yl}-N-{1-(3-chlorophenyl)-2-hydroxyethyl}-1H-pyrrole-2-carboxamide (*Lead 6: 35659*), 3-(4-(1H-indazol-5-ylamino)pyrimidin-2-ylamino) benzamide (*Lead 7: 26171*),(S)-4-{2-(4-Chloro-2-fluorophenylamino)-5-methylpyrimidin-4-yl}-N-{1-(3-chlorophenyl)-2-hydroxyethyl}-1H-pyrrole-2-carboxamide (*Lead 8: 35658*), [4-chloro-3-(4-methylpiperazin-1-ylmethyl) phenyl]-[5-(2-methylamino-pyrimidin-4-yloxy)-1H-benzimidazol-2-yl]-amine (*Lead 9: 17692*), 3-(4-(3H-benzo[d][1,2,3]triazol-5-ylamino)pyrimidin-2-ylamino)benzamide (*Lead 10: 26173*), N′-(3-methyl-2H-indazol-6-yl)-N-(3,4,5-trimethoxyphenyl) pyrimidine -2,4-diamine N4-(3-Methyl-1H-indazol-6-yl)-N2-[3,4,5-tris(methyloxy)phenyl]-2,4-pyrimidinediamine (*Lead 11: 26479*), 8-Cyclopentyl-2-(3-fluoro-4-piperazin-1-yl-phenylamino)-quinazolin-7-ol (*Lead 12: 6348*), and 8-Cyclopentyl-2-(4-piperazin-1-yl-phenylamino)-quinazolin-7-ol (*Lead 13: 6347*). The chemical structures of these lead molecules are illustrated in Fig. 3. The structural scaffold of the lead molecules contains amino functional group, mainly responsible for the hydrogen bond(s) formed with the JAK2. PRIME MM/GBSA solvation energy (ΔG_{bind}) was ranging from −2.00 to −77.00 kcal/mol and favorable binding *G*-score (−12.688 to −13.869) (Table 7) suggest strong ligand enzyme interactions. Azd1480, a potential JAK2 inhibitor [36] was included in the high throughput virtual screening procedure as a reference compound. Azd1480 is also binding in the same binding pocket of JAK2 with the docking score of −9.186 and ΔG_{bind} of −66.894 kcal/mol.

3.6. Biological activity predictions

In PASS, chemical structure is described by original descriptors called multilevel neighborhoods of atoms (MNA). MNA descriptors are rather universal and are capable of representing various structure–property relationships, including many types of biological activity, mutagenicity and carcinogenicity, drug likeness, and others [37,38]. Based on the statistics of MNA descriptors for active and inactive compounds from the original training set, two probabilities are calculated for each activity: *Pa* – the probability of the compound being active and *Pi* – the probability of being inactive. The *Pa* and *Pi* values vary from 0 to 1, and $Pa + Pi < 1$, since these probabilities are calculated independently. *Pa* and *Pi* can be considered to be measures of the compound under study belonging to the classes of active and inactive compounds, respectively [37]. The most probable activities for a given compound are characterized by *Pa* values close to 1, and *Pi* values close to 0 [31]. PASS prediction of lead 1, lead 2, lead 4, lead 6 and lead 8 shows activity against Janus tyrosine kinase. Their *Pa* values are 0.725, 0.653, 0.696, 0.738, 0.426 and *Pi* values are 0.002, 0.002, 0.002, 0.002 and 0.004 respectively.

3.7. Analysis of atom-based PHASE 3D-QSAR model

Additional inside into the inhibitory activity can be gained by visualizing the QSAR model in the context of most active and least active compounds. The contribution maps obtained from Hypothesis 1 shows how 3D-QSAR methods can identify features important for the interaction between ligands and their target protein. Such maps allow identification of those positions that require a particular physicochemical property to enhance the bioactivity of a ligand. A pictorial representation of the contours generated is shown in Fig. 4a–f. In these representations, the blue cubes indicate favorable regions while red cubes indicate unfavorable regions for activity.

Fig. 4a and b compares the most significant favorable and unfavorable electron withdrawing features that arise when the QSAR model is applied to the most active compound 21 and least active compound 31. The blue cubes are observed near the methansulfonamide and thiomorpholine dioxide moiety of compound 21 suggests that these features are important for the activity of the molecule and these functional groups should be unsubstituted. In compound 31 red cubes were observed in morpholine and two methyl groups in methylpropanenitrile. Substitution of morpholine to thiomorpholine dioxide and substitution of methylpropanenitrile with methansulfonamide increase the activity of compound 21.

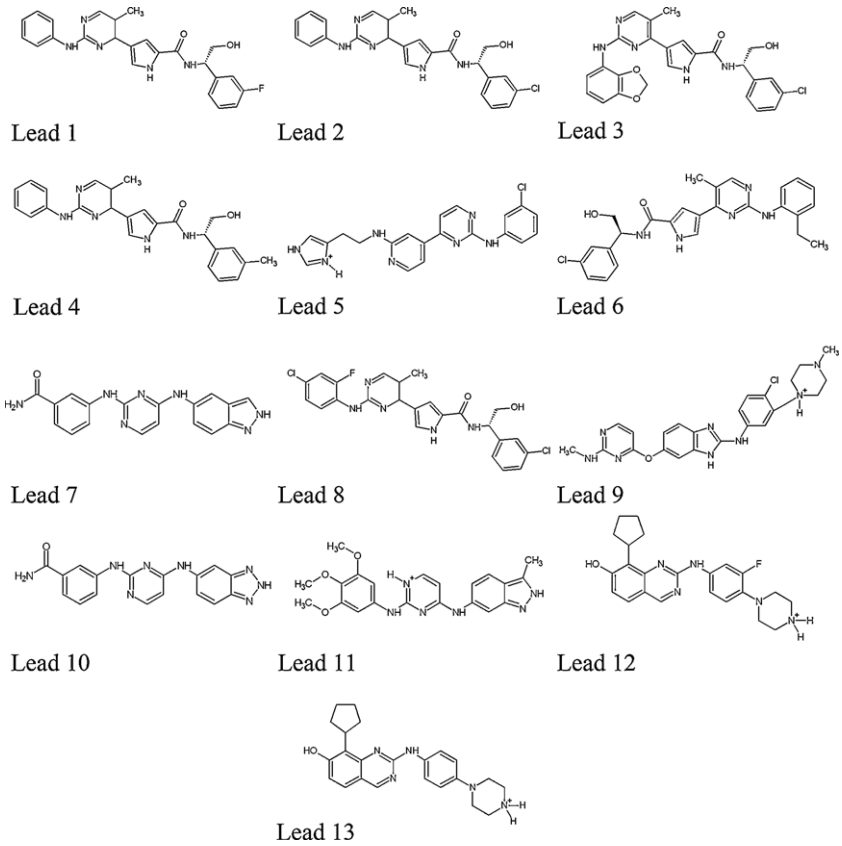

Fig. 3. Structures of the thirteen lead molecules.

We also examined the QSAR model of a compound with best pharmacokinetic properties (compound 28). It was observed that the two methyl groups were removed from the methylpropanenitrile moiety of compound 31 and it increases the activity and pharmacokinetic property as it is observed in compound 28 (Fig. 4c). Hence, thiomorpholine dioxide is important for the activity of the compounds.

Fig. 4d and e compare the most significant favorable and unfavorable hydrogen bond donor that arise when the QSAR model is applied to the most active compound 21 and least active compound 31. Blue cubes where observed near the nitrogen of thiomorpholine dioxide, indicating their importance for activity in context to compound 21, which again clearly shows thiomorpholine dioxide substitution is important for the activity. Blue cubes were absent in morpholine moiety in context to compound 31 and compound 28 (Fig. 4f).

The most significant favorable and unfavorable hydrophobic interaction that arise when the QSAR model is applied to the most active compound 21 and least active compound 31 (Supplementary Fig. 1a and b). Blue cubes were observed in most region of the compound in context to compound 21 while red cubes were observed in methylpropanenitrile moiety and morpholine moiety when observed in context to compound 31. Again, when the QSAR model was observed in context to compound 28, red cubes were

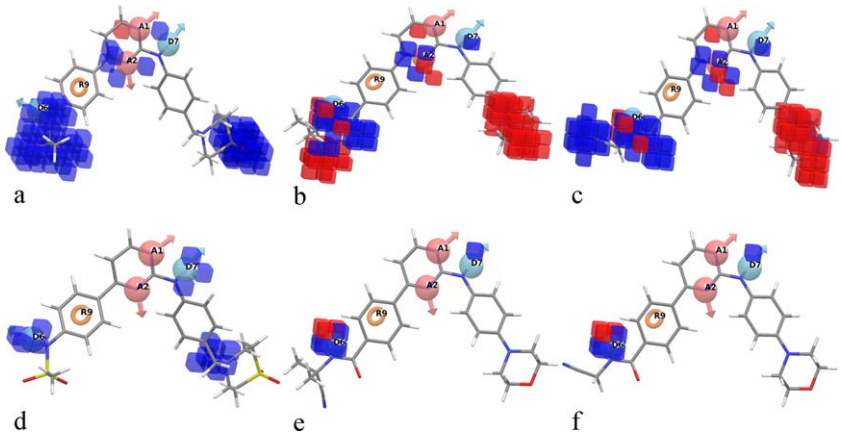

Fig. 4. Pictorial representation of the cubes generated using the QSAR model. Light grey indicate favorable regions while dark grey indicates unfavorable region for the activity. QSAR model visualized in the context of electron withdrawing features with most active compound 21(a), least active compound 31(b) and best pharmacokinetic compound 28(c). QSAR model visualized in the context of favorable and unfavorable hydrogen bond donor with most active molecule 21(d), least active compound 31(e) and best pharmacokinetic compound 28(f).

mainly observed near the N-(cyanomethyl) formamide moiety (Supplementary Fig. 1c). These clearly explain that methansulfonamide and thiomorpholine dioxide substitution increase the activity of the compounds.

3.8. Binding mode analysis of most active compound 21, least active compound 31 and best pharmacokinetic compound 28

Molecular docking studies were performed to understand the binding mode of the active compounds 21, 31 and 28 on JAK2 active site and to obtain information for further structure optimization, we have used extra precision glide docking (Glide XP) which docks ligands flexibly. The docking analysis of compound 21 at JAK2 active site shows the following interactions (Supplementary Fig. 2): thiomorpholine dioxide interacts with Asp939, methansulfonamide interacts with Asp994 and nitrogen from the pyrimidine and amine group interacts with Leu932. Methansulfonamide and thiomorpholine dioxide are located in the solvent exposed area. As explain before, due to the addition of oxosulfane oxide in the cyclohexane, one hydrogen bond donating group is created and make an interaction with Asp939. This complies with our developed atom based 3D-QSAR model. The docking analysis of compound 31 at JAK2 active site shows following interactions (Supplementary Fig. 2b): the hydrocyanic acid group interacts with Arg980, nitrogen from the pyrimidine and amine group interacts with Leu932. Due to the addition of two methy groups in N-(cyanomethyl) formamide moiety amino group fails to interact with the Asp994, which can account for low activity for compound 31. The docking analysis of compound 28 shows the following interactions (Supplementary Fig. 2c): the hydrocyanic acid group and amino group from N-(cyanomethyl) formamide moiety make an interaction with Arg980 and Asp994 respectively. Nitrogen from the pyrimidine and amine group also interacts with Leu932. From the figure it also shows that N-(cyanomethyl) formamide moiety occupy the maximum solvent expose area and embedded deep inside the active pocket. The docking results highlight that substitution of thiomorpholine dioxide in compound 28 lost an interaction with Asp939 but substitution of methansulfonamide to N-(Cynanomethyl) formamide shows additional interaction with Arg980. Thus, it shows that the substitution of N-(cyanomethy) formamide and thiomorpholine to the 4-phenyl-N-[4-(piperidin-1-yl)phenyl]pyrimidin-2-amine scaffold will increase the activity and pharmacokinetic property of the compound. PRIME MM/GBSA solvation energy (ΔG_{bind}) for compound 21 was also found to be −74.759 kcal/mol, −10.412 kcal/mol for compound 28 kcal/mol and 0.614 for compound 31. Docking score and binding energy of compounds selected for QSAR study are shown in Table 8.

3.9. Predicted ADME properties

We analyzed 44 physically significant descriptors and pharmaceutically relevant properties of 13 lead compounds, among which were molecular weight, H-bond donors, H-bond acceptors, log *p*, log p MDCK, log Kp, humoral absorption according to Lipinski's rule of 5 (Table 9 and Supplementary Table 3). Lipinski's rule of 5 is a rule of thumb to evaluate drug likeness, or determine if a chemical compound with a certain pharmacological or biological activity has properties that would make it a likely orally active drug in humans. The rule describes molecular properties important for a drug's pharmacokinetics in the human body, including its ADME. These compounds were further evaluated for their drug-like behavior through analysis of pharmacokinetic parameters required for absorption, distribution, metabolism and excretion (ADME) by use of QikProp [32,39]. For the 13 lead compounds, the partition coefficient (QPlogPo/w) and water solubility (QPlogS), critical for estimation of absorption and distribution of drugs within the body ranged between 0.8 to 5.3 and −8.092 to −3.102. Cell permeability (QPPCaco), a key factor governing drug metabolism and its access to biological membranes, ranged from 62.460 to 812.195, QPPMDCK ranges from 24.691 to 2955.977. Overall, the percentage human oral absorption for the compounds ranged from 73.555 to 100%. All these pharmacokinetic parameters are within the acceptable range defined for human use (see Table 9 footnote), thereby indicating their potential as drug-like molecules.

4. Conclusion

Different pharmacophore hypotheses of phenylaminopyrimidines derivatives as inhibitors of Janus kinases (JAK2) were developed using PHASE, and alignment based on these pharmacophores was used as the input for the development of 3D-QSAR models. A five point pharmacophore with two hydrogen bond acceptors (A), two hydrogen bond donors (D) and one aromatic ring (R) as pharmacophore features was associated with a 3D-QSAR model with good statistical significance and good predictive ability. Hypothesis 1 was significantly more accurate than other models, with good $R^2 = 0.970$, $Q^2 = 0.822$. Further, visualization of the 3D-QSAR model in the context of the molecules under study provided details of the relationship between structure and activity, and thus provides explicit indications for the design of better analogues. The result reveals that methansulfonamide and thiomorpholine dioxide substitution enhance the activity of the compounds. In addition, a molecular docking approach was applied to verify the pharmacophore and 3D-QSAR model developed. The docking results highlight that substitution of thiomorpholine dioxide in compound 28 lost an interaction with Asp939 but substitution of methansulfonamide to N-(Cynanomethyl) formamide shows additional interaction with Arg980. Thus, it concluded that the substitution of N-(cyanomethy) formamide and thiomorpholine to the 4-phenyl-N-[4-(piperidin-1-yl) phenyl] pyrimidin-2-amine scaffold will enhance the activity and pharmacokinetic property of the compound. Then, the pharmacophore model was employed as 3D search query to screen against public compound libraries. The pharmacophore captured more than 1000 hits which were filtered by three docking runs, identifying 13 hits. All these were predicted as high active 3D-QSAR model and showed the highest docking scores. In summary, ligand based 3D-QSAR model presented in this study based on pharmacophore conformations could be very useful for lead optimization. Interestingly, some of the compounds showed activity against JAK2 by PASS biological activity prediction. Moreover structure base screening of compounds further refined and optimized the lead compounds.

Appendix A. Supplementary data

Supplementary data associated with this article can be found, in the online version, at doi:10.1016/j.jmgm.2011.07.004.

References

[1] T.A. Wallace, S.L. Xia, P.P. Sayeski, Jak2 tyrosine kinase prevents angiotensin II-mediated inositol 1,4,5-trisphosphate receptor degradation, Vasc. Pharmacol. 43 (2005) 336–345.
[2] I.S. Lucet, E. Fantino, M. Styles, R. Bamert, O. Patel, S.E. Broughton, M. Walter, C.J. Burns, H. Treutlein, A.F. Wilks, J. Rossjohn, The structural basis of Janus kinase 2 inhibition by a potent and specific pan-Janus kinase inhibitor, Blood 107 (2006) 176–183.
[3] I. McDoom, X. Ma, A. Kirabo, K.-Y. Lee, D.A. Ostrov, P.P. Sayeski, Identification of tyrosine 972 as a novel site of Jak2 tyrosine kinase phosphorylation and its role in Jak2 activation, Biochemistry 47 (2008) 8326–8334.
[4] S. Ioannidis, M.L. Lamb, A.M. Davies, L. Almeida, M. Su, G. Bebernitz, M. Ye, K. Bell, M. Alimzhanov, M. Zinda, Discovery of pyrazol-3-ylamino pyrazines as novel JAK2 inhibitors, Bioorg. Med. Chem. Lett. 19 (2009) 6524–6528.

[5] S. Antonysamy, G. Hirst, F. Park, P. Sprengeler, F. Stappenbeck, R. Steensma, M. Wilson, M. Wong, Fragment-based discovery of JAK-2 inhibitors, Bioorg. Med. Chem. Lett. 19 (2009) 279–282.
[6] N.K. Williams, R.S. Bamert, O. Patel, C. Wang, P.M. Walden, A.F. Wilks, E. Fantino, J. Rossjohn, I.S. Lucet, Dissecting specificity in the Janus kinases: the structures of JAK-specific inhibitors complexed to the JAK1 and JAK2 protein tyrosine kinase domains, J. Mol. Biol. 387 (2009) 219–232.
[7] E. Mercier, G.r. Lissalde-Lavigne, J.-C. Gris, JAK2 V617F mutation in unexplained loss of first pregnancy, N. Engl. J. Med. 357 (2007) 1984–1985.
[8] C. Tono, G. Xu, T. Toki, Y. Takahashi, S. Sasaki, K. Terui, E. Ito, JAK2 Val617Phe activating tyrosine kinase mutation in juvenile myelomonocytic leukemia, Leukemia 19 (2005) 1843–1844.
[9] E. Chen, P.A. Beer, A.L. Godfrey, C.A. Ortmann, J. Li, A.P. Costa-Pereira, C.E. Ingle, E.T. Dermitzakis, P.J. Campbell, A.R. Green, Distinct clinical phenotypes associated with JAK2V617F reflect differential STAT1 signaling, Cancer Cell 18 (2010) 524–535.
[10] R. Kralovics, F. Passamonti, A.S. Buser, S.-S. Teo, R. Tiedt, J.R. Passweg, A. Tichelli, M. Cazzola, R.C. Skoda, A gain-of-function mutation of JAK2 in myeloproliferative disorders, N. Engl. J. Med. 352 (2005) 1779–1790.
[11] M.W. Ledeboer, A.C. Pierce, J.P. Duffy, H. Gao, D. Messersmith, F.G. Salituro, S. Nanthakumar, J. Come, H.J. Zuccola, L. Swenson, D. Shlyakter, S. Mahajan, T. Hoock, B. Fan, W.-J. Tsai, E. Kolaczkowski, S. Carrier, J.K. Hogan, R. Zessis, S. Pazhanisamy, Y.L. Bennani, 2-Aminopyrazolo[1,5-a]pyrimidines as potent and selective inhibitors of JAK2, Bioorg. Med. Chem. Lett. 19 (2009) 6529–6533.
[12] P. Peeters, S.D. Raynaud, J. Cools, I. Wlodarska, J. Grosgeorge, P. Philip, F. Monpoux, L. Van Rompaey, M. Baens, H. Van den Berghe, P. Marynen, Fusion of TEL, the ETS-variant gene 6 (ETV6), to the receptor-associated kinase JAK2 as a result of t(9; 12) in a lymphoid and t(9; 15; 12) in a myeloid leukemia, Blood 90 (1997) 2535–2540.
[13] R.L Levine, M. Carroll, A common genetic mechanism in malignant bone marrow diseases, N. Engl. J. Med. 360 (2009) 2355–2357.
[14] S. Takemoto, J.C. Mulloy, A. Cereseto, T.-S. Migone, B.K.R. Patel, M. Matsuoka, K. Yamaguchi, K. Takatsuki, S. Kamihira, J.D. White, W.J. Leonard, T. Waldmann, G. Franchini, Proliferation of adult T cell leukemia/lymphoma cells is associated with the constitutive activation of JAK/STAT proteins, Proc. Natl. Acad. Sci. U. S. A. 94 (1997) 13897–13902.
[15] G.W. Booz, J.N.E. Day, R. Speth, K.M. Baker, Cytokine G-protein signaling crosstalk in cardiomyocytes: attenuation of Jak-STAT activation by endothelin-1, Mol. Cell. Biochem. 240 (2002) 39–46.
[16] C. Guilluy, J. Bregeon, G. Toumaniantz, M. Rolli-Derkinderen, K. Retailleau, L. Loufrani, D. Henrion, E. Scalbert, A. Bril, R.M. Torres, S. Offermanns, P. Pacaud, G. Loirand, The Rho exchange factor Arhgef1 mediates the effects of angiotensin II on vascular tone and blood pressure, Nat. Med. 16 (2010) 183–190.
[17] R. Kiss, T. Polgár, A. Kirabo, J. Sayyah, N.C. Figueroa, A.F. List, L. Sokol, K.S. Zuckerman, M. Gali, K.S. Bisht, P.P. Sayeski, G.M. Keseru, Identification of a novel inhibitor of JAK2 tyrosine kinase by structure-based virtual screening, Bioorg. Med. Chem. Lett. 19 (2009) 3598–3601.
[18] N. Tawari, S. Bag, M. Degani, Pharmacophore mapping of a series of pyrrolopyrimidines, indolopyrimidines and their congeners as multidrug-resistance-associated protein (MRP1) modulators, J. Mol. Model. 14 (2008) 911–921.
[19] S. Dixon, A. Smondyrev, E. Knoll, S. Rao, D. Shaw, R. Friesner, PHASE: a new engine for pharmacophore perception, 3D QSAR model development, and 3D database screening: 1. Methodology and preliminary results, J. Comput. Aided Mol. Des. 20 (2006) 647–671.
[20] Phase 3.2. Schrödinger, LLC, New York, NY, 2010.
[21] S.L. Dixon, A.M. Smondyrev, S.N. Rao, PHASE: a novel approach to pharmacophore modeling and 3D database searching, Chem. Biol. Drug Des. 67 (2006) 370–372.
[22] C.J. Burns, D.G. Bourke, L. Andrau, X. Bu, S.A. Charman, A.C. Donohue, E. Fantino, M. Farrugia, J.T. Feutrill, M. Joffe, M.R. Kling, M. Kurek, T.L. Nero, T. Nguyen, J.T. Palmer, I. Phillips, D.M. Shackleford, H. Sikanyika, M. Styles, S. Su, H. Treutlein, J. Zeng, A.F. Wilks, Phenylaminopyrimidines as inhibitors of Janus kinases (JAKs), Bioorg. Med. Chem. Lett. 19 (2009) 5887–5892.
[23] V. Lather, R. Kristam, J.S. Saini, N.A. Karthikeyan, V.N. Balaji, QSAR models for prediction of glycogen synthase kinase-3β inhibitory activity of indirubin derivatives, QSAR Comb. Sci. 27 (2008) 718–728.
[24] X. Pan, N. Tan, G. Zeng, H. Huang, H. Yan, 3D QSAR studies on ketoamides of human cathepsin K inhibitors based on two different alignment methods, Eur. J. Med. Chem. 45 (2010) 667–681.
[25] A. Golbraikh, A. Tropsha, Beware of q^2!, J. Mol. Graph. Model. 20 (2002) 269–276.
[26] P. Lu, X. Wei, R. Zhang, CoMFA and CoMSIA 3D-QSAR studies on quionolone caroxylic acid derivatives inhibitors of HIV-1 integrase, Eur. J. Med. Chem. 45 (2010) 3413–3419.
[27] A. Basu, K. Jasu, V. Jayaprakash, N. Mishra, P. Ojha, S. Bhattacharya, Development of CoMFA and CoMSIA models of cytotoxicity data of anti-HIV-1-phenylamino-1H-imidazole derivatives, Eur. J. Med. Chem. 44 (2009) 2400–2407.
[28] T.A. Halgren, R.B. Murphy, R.A. Friesner, H.S. Beard, L.L. Frye, W.T. Pollard, J.L. Banks, Glide: a new approach for rapid, accurate docking and scoring. 2. Enrichment factors in database screening, J. Med. Chem. 47 (2004) 1750–1759.
[29] M. Afroz Alam, P. Naik, Molecular modelling evaluation of the cytotoxic activity of podophyllotoxin analogues, J. Comput. Aided Mol. Des. 23 (2009) 209–225.
[30] A. Lagunin, A. Stepanchikova, D. Filimonov, V. Poroikov, PASS: prediction of activity spectra for biologically active substances, Bioinformatics 16 (2000) 747–748.
[31] V.V. Poroikov, D.A. Filimonov, W.-D. Ihlenfeldt, T.A. Gloriozova, A.A. Lagunin, Y.V. Borodina, A.V. Stepanchikova, M.C. Nicklaus, PASS biological activity spectrum predictions in the enhanced open NCI database browser, J. Chem. Inf. Model. 43 (2002) 228–236.
[32] QikProp, version 3.3, Schrödinger, LLC, New York, NY, 2010.
[33] C.A. Lipinski, F. Lombardo, B.W. Dominy, P.J. Feeney, Experimental and computational approaches to estimate solubility and permeability in drug discovery and development settings, Adv. Drug Deliv. Rev. 46 (2001) 3–26.
[34] Y. Li, Y. Wang, F. Zhang, Pharmacophore modeling and 3D-QSAR analysis of phosphoinositide 3-kinase p110α inhibitors, J. Mol. Model. 16 (2010) 1449–1460.
[35] A. Tropsha, Best practices for QSAR model development, validation, and exploitation, QSAR Comb. Sci. 29 (2010) 476–488.
[36] S. Ioannidis, M.L. Lamb, T. Wang, L. Almeida, M.H. Block, A.M. Davies, B. Peng, M. Su, H.-J. Zhang, E. Hoffmann, C. Rivard, I. Green, T. Howard, H. Pollard, J. Read, M. Alimzhanov, G. Bebernitz, K. Bell, M. Ye, D. Huszar, M. Zinda, Discovery of 5-chloro-N2-[(1S)-1-(5-fluoropyrimidin-2-yl)ethyl]-N4-(5-methyl-1H-pyrazol-3-yl)pyrimidine-2,4-diamine (AZD1480) as a novel inhibitor of the Jak/Stat pathway, J. Med. Chem. 54 (2011) 262–276.
[37] K. Dhanachandra Singh, M. Karthikeyan, P. Kirubakaran, V. Sathya, S. Nagamani, Structure-based drug discovery of ApoE4 inhibitors from the plant compounds, Med. Chem. Res. (2010) 1–9, doi:10.1007/s00044-011-9595-3.
[38] C.H.T.d.P. da Silva, V.B. da Silva, J. Resende, P.F. Rodrigues, F.C. Bononi, C.G. Benevenuto, C.A. Taft, Computer-aided drug design and ADMET predictions for identification and evaluation of novel potential farnesyltransferase inhibitors in cancer therapy, J. Mol. Graph. Model. 28 (2010) 513–523.
[39] K.D. Singh, P. Kirubakaran, S. Nagarajan, S. Sakkiah, K. Muthusamy, D. Velmurgan, J. Jeyakanthan, Homology modeling, molecular dynamics, e-pharmacophore mapping and docking study of Chikungunya virus nsP2 protease, J. Mol. Model. (2011), 1–13, doi:10.1007/s00894-011-1018-3.